HORuS transmission spectroscopy of 55 Cnc e

H. M. Tabernero [1,2]★ C. Allende Prieto,[3,4] M. R. Zapatero Osorio,[2] J. I. González Hernández,[3,4]
C. del Burgo,[4,5] R. García López,[3,4] R. Rebolo,[3,4] M. Abril-Abril,[6] R. Barreto,[3,4] J. Calvo Tovar,[3,4]
A. Díaz Torres,[3,4] P. Fernández Izquierdo,[3,4] M. F. Gómez-Reñasco,[3,4] F. Gracia-Témich,[3,4] E. Joven,[3,4]
J. Peñate Castro,[3,4] S. Santana-Tschudi,[3,4] F. Tenegi[3,4] and H. D. Viera Martín[6]

[1]*Instituto de Astrofísica e Ciências do Espaço, Universidade do Porto, CAUP, Rua das Estrelas, P-4150-762 Porto, Portugal*
[2]*Centro de Astrobiología (CSIC-INTA), Carretera de Ajalvir km 4, Torrejón de Ardoz, E-28850 Madrid, Spain*
[3]*Dpto. Astrofísica, Universidad de La Laguna, E-38206 La Laguna, Tenerife, Spain*
[4]*Instituto de Astrofísica Canarias, vía Láctea s/n, E-38205 La Laguna, Tenerife, Spain*
[5]*Instituto Nacional de Astrofísica, Óptica y Electrónica, Luis Enrique Erro 1, Sta. Ma. Tonantzintla, 72840 Puebla, Mexico*
[6]*Gran Telescopio Canarias, Cuesta de San José s/n, E-38712 Breña Baja, La Palma, Spain*

ABSTRACT

The High Optical Resolution Spectrograph (HORuS) is a new high-resolution echelle spectrograph available on the 10.4-m Gran Telescopio Canarias (GTC). We report on the first HORuS observations of a transit of the super-Earth planet 55 Cnc e. We investigate the presence of Na I and Hα in its transmission spectrum and explore the capabilities of HORuS for planetary transmission spectroscopy. Our methodology leads to residuals in the difference spectrum between the in-transit and out-of-transit spectra for the Na I doublet lines of $(3.4 \pm 0.4) \times 10^{-4}$, which sets an upper limit to the detection of line absorption from the planetary atmosphere that is one order of magnitude more stringent that those reported in the literature. We demonstrate that we are able to reach the photon-noise limit in the residual spectra using HORuS to a degree that we would be able to easily detect giant planets with larger atmospheres. In addition, we modelled the structure, chemistry, and transmission spectrum of 55 Cnc e using state-of-the-art open source tools.

Key words: planets and satellites: atmospheres – planets and satellites: individual: 55 Cnc e.

1 INTRODUCTION

Planets orbiting stars are ubiquitous, as demonstrated by more than 4000 planets discovered to date.[1] With the pace of exoplanetary discoveries still increasing thanks to multiple transiting and radial velocity surveys carried out with e.g. space missions like the *Kepler, K2, CoRoT*, and *TESS* (Ricker 2014); the ground-based spectrographs such as HARPS (Mayor et al. 2003), HARPS-N (Cosentino et al. 2012), HIRES (Vogt et al. 1994), CARMENES (Quirrenbach et al. 2016), and MARVELS (Alam et al. 2015); and new and future instruments like ESPRESSO (Pepe et al. 2010), *CHEOPS* (Rando et al. 2018), HPF (Mahadevan et al. 2014), *JWST* (Gardner et al. 2006), *PLATO* (Rauer et al. 2014), NIRPS (Wildi et al. 2017), and SPIRou (Moutou et al. 2015). Exoplanetary research is now approaching the deep study and characterization of the atmospheres of the extrasolar planets.

Transiting exoplanets present a unique opportunity to characterize their atmospheres, and learn about their chemical composition. Charbonneau et al. (2002) reported the first detection of an exoplanet atmosphere by means of *Hubble Space Telescope* spectroscopy. These authors detected the resonance doublet of Na I in the Jupiter-size planet HD 209458 b. Casasayas-Barris et al. (2020) showed that this detection is due to the Rossiter–Mclaughlin (RM) effect and not to the atmosphere of the planet. In spite of that result, Charbonneau et al. (2002) opened a new era in the study of exoplanets. The first detection of an exoplanet atmosphere with a ground-based telescope was made by Redfield et al. (2008), who identified the absorption of the sodium resonance lines caused by the atmosphere of HD 189733 b. Line absorption of Na, K, He, CO, CH$_4$, or water vapour has already been reported in the atmospheres of tens of giant gaseous planets (e.g. Barman et al. 2015; Allart et al. 2017; Sheppard et al. 2017; Chen et al. 2018; Nortmann et al. 2018; Parmentier et al. 2018; Alonso-Floriano et al. 2019; Seidel et al. 2019). In addition, atomic absorption features due to Fe I,II and Ti I,II have been detected in the atmosphere of the ultrahot Jupiter KELT-9 b (Hoeijmakers et al. 2018, 2019). These measurements represent a step forward in our understanding of the chemistry of planetary atmospheres and our ability to constrain planet formation theories. The study of exoplanetary atmospheres is also moving towards the exploration of the atmospheres of rocky planets (i.e. super-Earths), but these atmospheres are harder to detect.

Spectroscopy is a powerful tool used to detect both broad and narrow features in the transmission spectra of transiting exoplanets, all of which are important ingredients to unveil their chemistry. The High Optical Resolution Spectrograph (HORuS) at the Gran Telescopio Canarias (GTC) offers an excellent opportunity for this task, given its moderate spectral resolution ($R \approx 25\,000$) at optical wavelengths, and large collecting area, which is critical for achieving

★ E-mail: htabernero@astro.up.pt
[1]https://exoplanetarchive.ipac.caltech.edu

Table 1. Orbital and physical parameters for 55 Cnc and 55 Cnc e.

Parameter	Value	Reference
Stellar properties		
T_{eff}	5353 ± 62 K	Sousa et al. (2018)
$\log g$	4.30 ± 0.14 dex	Sousa et al. (2018)
[Fe/H]	0.30 ± 0.04 dex	Sousa et al. (2018)
ξ	1.01 ± 0.10 km s^{-1}	Sousa et al. (2018)
M_*	0.97 ± 0.09 M$_\odot$	Bourrier et al. (2018)
R_*	1.73 ± 0.04 R$_\odot$	Bourrier et al. (2018)
Planet properties		
P	0.7365474 ± 0.0000014 d	Bourrier et al. (2018)
M_p	7.99 ± 0.33 M$_\oplus$	Bourrier et al. (2018)
R_p	1.875 ± 0.05 R$_\oplus$	Bourrier et al. (2018)
K_1	6.02 ± 0.24 m s^{-1}	Bourrier et al. (2018)
a	0.01544 ± 0.00005 au	Bourrier et al. (2018)
γ	27.45145 ± 0.00089 km s^{-1}	Bourrier et al. (2018)
e	0.05 ± 0.03	Bourrier et al. (2018)
ω	$86°0^{+30°7}_{-33°4}$	Bourrier et al. (2018)

a high signal-to-noise ratio (S/N) during the limited time window of the planetary transit.

In this work, we analyse the HORuS commissioning data for a single transit of the hot and dense super-Earth planet 55 Cnc e, which is orbiting one of the brightest planet-host stars known to have a super-Earth planet (Bourrier et al. 2018). The 55 Cnc system is an interesting multiplanetary system with five known planets that have been discovered during the last decades (see Butler et al. 1997; Marcy et al. 2002; McArthur et al. 2004; Fischer et al. 2008). 55 Cnc e is a super-Earth planet of mass 7.99 M$_\oplus$ and a planetary radius of 1.875 R$_\oplus$. It orbits its parents star with a short period of $\approx$0.7 d at a distance to the host star 55 Cnc of 0.01 au. This paper consists of the following sections. The HORuS observations and data reduction procedure are described in Section 2. The extraction of the planetary signal is documented in Section 3. In Section 4, we discuss our results and compare them to those obtained in previous works. Finally, in Section 5, we present the impact of our findings, whereas the extra material is given in Fig. A1.

2 OBSERVATIONS

A series of spectroscopic observations covering one transit of the super-Earth 55 Cnc e (see Table 1) was obtained with HORuS,[2] which is a moderate-resolution echelle spectrograph ($R \approx 25\,000$) in operation at the 10.4-m GTC. It collects light at the Nasmyth-B focal plane, shared with OSIRIS, using a 3×3 integral field unit (IFU, 2.1×2.1 arcsec^2) with microlenses, into optical fibres that form a pseudo-slit at the spectrograph entrance, fitted with another set of microlenses. The light is dispersed with a 79 gr mm^{-1} echelle grating and cross-dispersed with three prisms, providing nearly continuous coverage between 3800 and 6900 Å split over 27 spectral orders. The detector is a 4096×4096 15-µm-pixel Fairchild CCD.

We observed one transit of 55 Cnc e using HORuS at the GTC during the night of 2018 December 12. This night and the preceding one were part of a commissioning run for HORuS. The CCD was read with no binning, and a readout time of 90 s. With a sampling of 6 pixels per resolution element in the spectral direction, and about the same number of pixels sampling each of the nine fibres in the IFU in the spatial direction, the 16-bit electronics can provide a maximum S/N of several thousand per exposure. We took spectra of the Th–Ar

hollow cathode for wavelength calibration during the transit, with a cadence of approximately 1 h. We obtained four 900-s exposures followed by twenty 450-s integrations, spanning slightly more than 4 h, and including the transit. Each 450-s exposure provided a S/N per resolution element in excess of 1800 at 550 nm, and about half of that at 420 nm. The observations span over $\approx$4.2 h, whereas the transit lasted for $\approx$1.6 h. A total of 10 spectra were acquired during the planetary transit of 55 Cnc e. In addition, we started observing at an airmass of 1.55, whereas the observations finished at an airmass of 1.05.

3 DATA ANALYSIS

3.1 Data reduction

The CHAIN,[3] a custom-made data reduction pipeline for HORuS written in IDL, was used to process the data, performing bias removal, finding, tracing, and extraction of the apertures corresponding to the spectral orders. Wavelength calibration involved fitting third- or fourth-order polynomials to one to two dozen thorium lines in each echelle order, identified in an atlas made with the Tull spectrograph (Allende Prieto 2001), and interpolating linearly the wavelength solutions between the Th and Ar exposures preceding and following each stellar spectrum. The collapse of the orders along the slit was done by adding the counts along the spatial direction of the detector. By taking ratios of two consecutive out-of-transit spectra we find that the distribution of the residuals for the central regions of the orders in the red part of the spectrum is well described by a Gaussian with a $\sigma \simeq 0.0018$, which is equivalent to a S/N per pixel of $\sqrt{2}/0.0018 \simeq 800$, or 1900 per resolution element, confirming the expectations based on the Poisson noise ($\sqrt{N_{counts}}$) for the accumulated stellar signal.

3.2 Instrumental corrections

Before attempting the extraction of the absorption signature imprinted by the planet's atmosphere in the spectrum of the star, we decided to analyse two particular spectral regions: the Na I doublet (5889.95 and 5895.92 Å) and the Hα line (6562.80 Å). HORuS is not stabilized thermally or mechanically, as it is the case of e.g. ESPRESSO (Pepe et al. 2010), HARPS (Mayor et al. 2003), and CARMENES (Quirrenbach et al. 2016). Consequently, variations in the point spread function of the instrument, inducing changes of up to 10 per cent in scales of hours, are typically found. We found that stability issues can be addressed by carefully aligning all the observed spectra by working in small wavelength regions of interest. Each individual spectroscopic observation has to be aligned with the others in terms of wave and flux. Spectral alignment is critical to extract the planetary signature, as the wavelength solution must be as precise as possible. To that aim, we generated an Fe I synthetic spectrum by means of TURBOSPECTRUM[4] (Plez 2012). In addition, we used a MARCS model atmosphere (Gustafsson et al. 2008) of $T_{eff} = 5250$ K, $\log g = 4.5$ dex, and [M/H] = 0.25 dex,[5] alongside an Fe I line list extracted from the Vienna Atomic Line Database 3 (VALD3; Ryabchikova et al. 2015). We adopted ISPEC (Blanco-Cuaresma et al. 2014) to cross-correlate each individual stellar observation with the generated Fe I synthetic spectrum. As a result we could measure the radial velocity corrections ($\sigma \approx 0.2$ km s^{-1}, see Table A1) required to shift each individual spectrum to the rest frame.
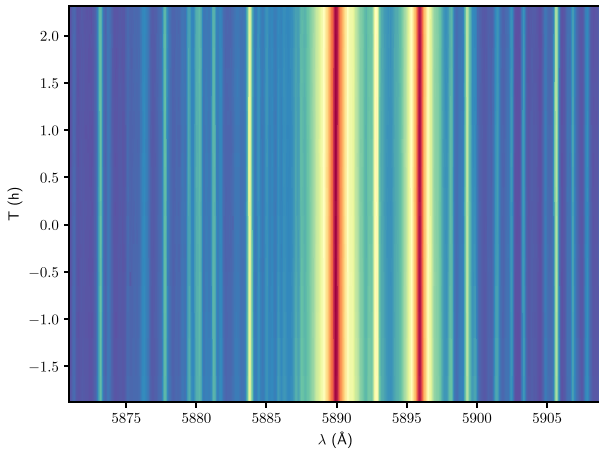
Figure 1. All HORuS spectra are shown vertically ordered in time (the earliest spectra are at the bottom). Time 0.0 h corresponds to the mid-transit according to the planetary ephemeris given in Table 1. The blue colour represents the continuum and all other colours stand for atomic absorption features (Na I doublet lines are the deepest). All stellar features are well aligned vertically and the flux continuum is nearly identical for all spectra.

Variations in the effective spectral resolution of HORuS also have to be taken into account to extract the planetary signal. Thus, we calculated a nominal resolution by measuring the width of Th lines in the calibration frames. The full width at half-maximum (FWHM) of the cross-correlation given by ISPEC of each individual Th–Ar exposure with itself (divided by $\sqrt{2}$) will give us an effective resolution for each exposure. At this point, we can homogenize all the observations to the exact same resolution, by means of convolving each spectrum with a Gaussian kernel that accounts for the missing broadening.

3.3 Extraction of the planetary signal

The flux changes from exposure to exposure due to variations in airmass and atmospheric transparency. Individual exposures must be corrected for these effects, and we used a low-order polynomial in order to have set of spectra in the same flux scale. The final result of flux alignment and wavelength correction is shown in Fig. 1. We separated the spectra into two categories, in-transit and out-of-transit spectra, by means of the ephemeris given by Bourrier et al. (2018). Then, we computed, wavelength by wavelength, the median of the out-of-transit spectra to generate a master spectrum. We employed the median to compute the out-of-transit spectrum because it is a non-skewed estimator more resilient to the influence of 'bad pixels' (i.e. cosmic rays) in an individual exposure. We can divide each observation by this master spectrum to get a set of residual spectra that can be later combined to extract the signature of the planetary transit.

The telluric correction was done in an iterative manner, since the wavelength ranges of interest to this work contain heavily blended telluric lines to correct for (as well as the instrument resolution). However, it is possible to correct them without completely removing the planetary signature. Thus, we decided to employ the SYSREM algorithm (Tamuz, Mazeh & Zucker 2005; Mazeh, Tamuz & Zucker 2007) to correct these lines. SYSREM is an iterative detrending algorithm that is used to remove artefacts in any set of residual spectra (after diving by the master spectrum). This algorithm has been successfully employed in the literature (e.g. Nugroho et al. 2017; Hawker et al. 2018; Alonso-Floriano et al. 2019) to retrieve

planetary signatures. We needed five SYSREM iterations to remove the remaining telluric residuals and achieving the photon-noise limit. This gives us a set of residual spectra clean of any tentative remaining stellar and telluric residuals. We can combine the in-transit spectra after correcting them for the velocity of the planet derived using the ephemeris given by Bourrier et al. (2018) (see Table 1). After all the residual in-transit spectra are shifted to the planet rest frame we can merge them (using a median, in a wavelength by wavelength basis) to extract the final planetary signal.

It is important to mention that SYSREM can partially remove the planet signal during each iteration. In consequence, we need to check that our method is not completely removing the planetary signal. Following Ridden-Harper et al. (2016) we injected a simulated planetary signal with an intensity of 0.005 to mimic the Na I lines. In Fig. 2, we show how our method does not remove any planetary signal, and that we can recover the injected model by means of only five SYSREM iterations. We performed the analysis described above for both Na I doublet and the Hα line, we retrieve an absorption depth at about $(4.1 \pm 0.3) \times 10^{-3}$ for both Na I lines. Whereas for Hα we retrieve a similar value of $(4.4 \pm 0.7) \times 10^{-3}$. In consequence, these two retrieved values reveal that SYSREM leaves the majority of the artificially injected planet signature intact.

4 DISCUSSION

The resulting planetary transmission spectrum centred at the resonance doublet of Na I and Hα is shown in Figs 3 and A2. We have not detected Na I in 55 Cnc e, as expected from its high mean molecular weight atmosphere contributing to only a small per cent of its planetary radius (Bourrier et al. 2018). However, we can infer an upper limit to the presence of these two lines. We have performed a bootstrap process to calculate the upper limit to the presence of the Na I and Hα lines. To that aim, we made groups of seven spectra to generate 120 transmission spectra in both spectral regions. Unfortunately, we have only a few observations and we had to make a compromise performing simulated spectra. Moreover, we need to allow variation to perform around 100 simulations without affecting the statistics of each individual simulation. All in all, thanks to these simulations we can calculate the accuracy achievable using HORuS data.

Our calculations gave us an upper limit of $(3.4 \pm 0.4) \times 10^{-4}$ to the presence of the Na I doublet lines. This value represents a factor of ≈ 10 improvement with respect to the previous measurements reported by Ridden-Harper et al. (2016). In addition, we have inferred an upper limit of $(7 \pm 1) \times 10^{-4}$ for the Hα line. The inferred upper limits are accurate to the first significant digit according to our bootstrap calculations. This is due to the relatively small number of statistically independent samples that can be drawn by means of the bootstrap method. The previous measurements in the Na I wavelength range were based on four transits of 55 Cnc e observed with HARPS/ESO 3.6 m and HARPS-N/TNG. Despite the non-detection of Na in 55 Cnc e, we have demonstrated that we are able to achieve the photon-noise limit of the exoplanetary data using HORuS to a degree that we will be able to detect giant planets. These planets have larger atmospheres and transmission depths above 10^{-3} (at the 3σ level) that can be easily detected, as indicated by our results.

In addition, our upper limit on Hα is in good agreement with the conclusions of Ehrenreich et al. (2012), as they do not detect any hints of neutral hydrogen in the transmission spectrum of 55 Cnc e. However, Tsiaras et al. (2016) detected two tentative HCN features in the infrared wavelength range (at 1.42 and 1.54 μm) suggesting a lightweight atmosphere.
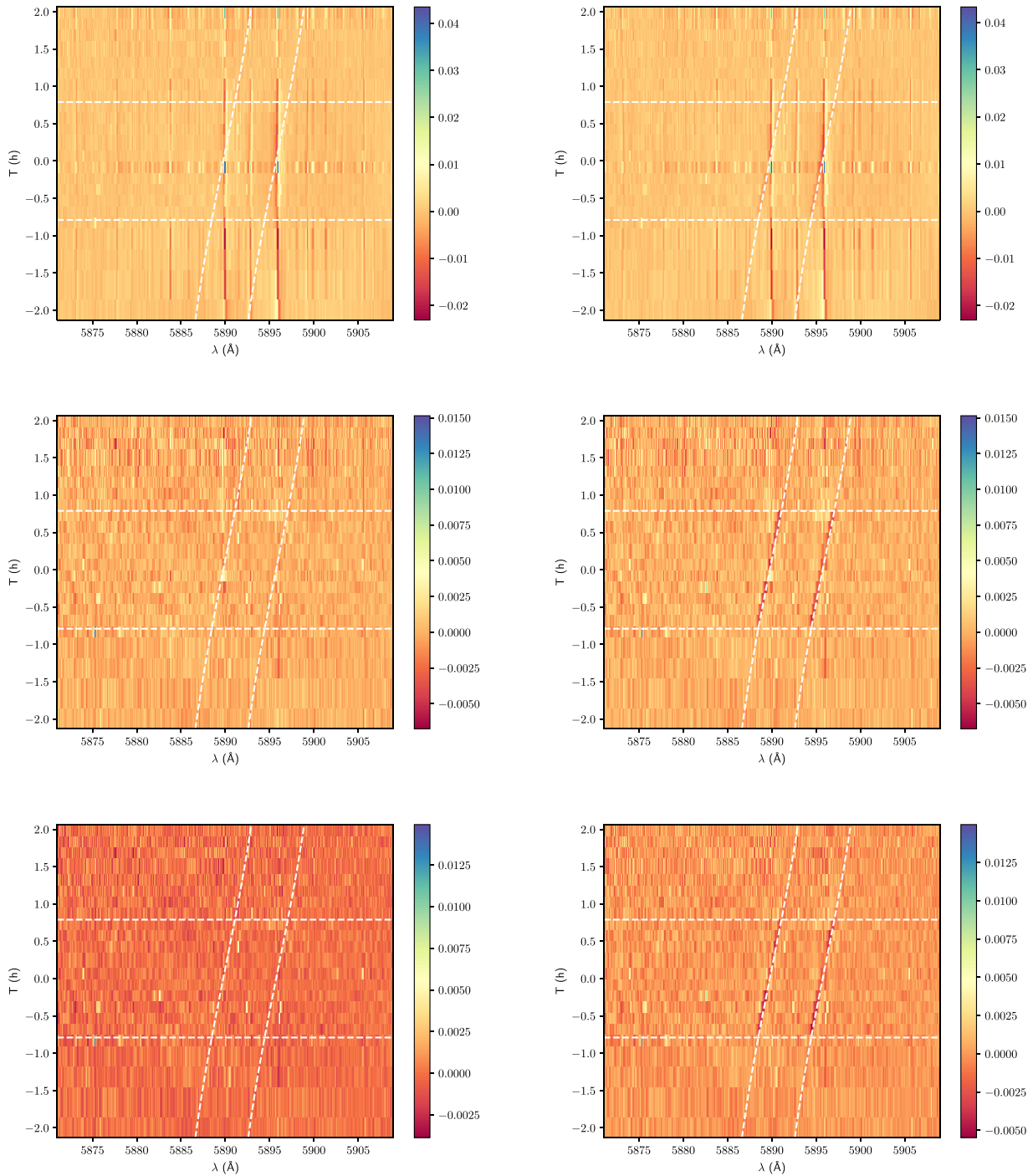
Figure 2. Visual representation of our SYSREM implementation applied to the Na I doublet. The left-hand column represents the HORuS data, whereas the right-hand column shows the same data with an injected planetary signal. Each row represents different steps of our SYSREM implementation. Here we represent our results for the removal of the master spectrum (top panels), as well as three and five SYSREM iterations. The transit window is given by the two horizontal dashed lines, whereas the planet trace is drawn by the two vertical curves.

Our estimated upper limit to the depth of the Na I doublet lines and Hα needs to be compared to the predictions of theoretical models. To that aim we computed an atmospheric structure using the HELIOS[6] code (see Figs A3 and A4; Malik et al. 2017, 2019). HELIOS allowed us to generate tailored models taking into account the irradiation of

the parent star. HELIOS requires fundamental parameters for both the star and the planet, as well as a chemical composition. Estimates for those parameters were taken from Bourrier et al. (2018), and we assumed solar abundances from Asplund et al. (2009). The HELIOS model was used in FASTCHEM[7] (Stock et al. 2018) to compute the

[6]https://github.com/exoclime/HELIOS

[7]https://github.com/exoclime/FastChem
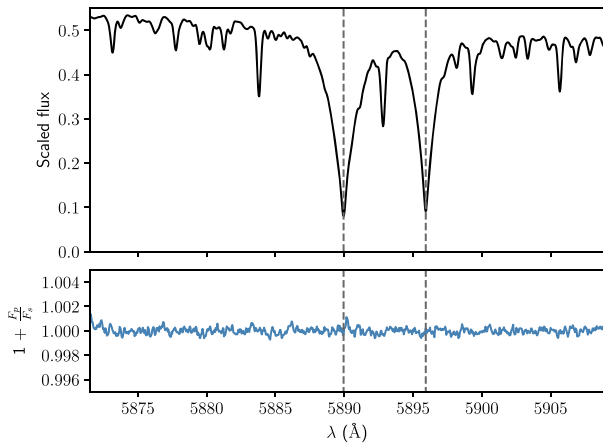
Figure 3. Final master stellar spectrum (top) and final transmission spectrum (bottom) for 55 Cnc e in the Na I region. The sodium doublet wavelengths are marked by the two vertical dashed lines.

number densities for several atomic and molecular species in the atmosphere of the planet (see Fig. A5). In addition, we calculated the transmission spectrum of 55 Cnc e thanks to the PETITRADTRANS[8] code (Mollière et al. 2019) alongside the HELIOS model and the particle number densities we have calculated with FASTCHEM. We used the high-resolution option of PETITRADTRANS to compute two synthetic spectra of 55 Cnc e using two different C/O ratios (solar and twice solar composition). The modelling of the planetary atmosphere is a necessary step to know what are the limits of HORuS. We plot these synthetic models in Fig. A6. Further inspection of our synthetic modelling reveals that the depths of the modelled sodium lines are $\approx 3 \times 10^{-5}$ with respect to the continuum. Therefore, we need to improve the noise level at least by a factor of 30 to be able to confidently detect any Na I in 55 Cnc e. Regarding Hα, our models are consistent with a non-detection of this feature at the resolution of HORuS independently of the C/O ratio (Fig. A6). Thus, ruling out atmospheres with lower mean molecular weight than those of our models requires a better S/N. In consequence, future observations with an improved S/N are required in order to be able to confidently detect (3σ detection) the atmosphere of 55 Cnc e.

5 CONCLUSIONS

In this work, we have analysed the transit of the super-Earth 55 Cnc e in the Na I doublet region to explore the capabilities of HORuS as a high-resolution echelle spectrograph. The main conclusions of this work can be summarized as follows.

(i) We estimated uncertainties in the derived radial velocities at about 0.2 km s^{-1}. This is typical for instruments like HORuS, which have not been stabilized thermally, optically, or mechanically.

(ii) We confirm that the high sampling of the signal provided by HORuS, with order widths of about 60 pixels in the spatial direction and 6 pixels in the spectral direction, can provide an S/N of about 1900 per resolution element in a single 450-s exposures for 55 Cnc.

(iii) Our methodology has allowed us to place a limit on the detection of the planetary signal in the by Na I resonance doublet of $(3.4 \pm 0.4) \times 10^{-4}$, improving by a factor of approximately 10, a previous limit given by Ridden-Harper et al. (2016).

(iv) We have also studied the noise level for the Hα line, proving a limit to the presence of Hα: $(7 \pm 1) \times 10^{-4}$.

(v) Our modelling indicated that the S/N of our observations has to be increased by a factor of 30 to detect the atmosphere of 55 Cnc e at the 3σ level.

(vi) We have demonstrated that we are able to reach the photon-noise limit of the exoplanetary data using HORuS to a degree that we can detect planets with larger atmospheres (i.e. giant planets). These planets will be easily detected, as indicated by the results of this study.

DATA AVAILABILITY

The data underlying this paper will be shared on reasonable request to the corresponding author.

REFERENCES

Alam S. et al., 2015, ApJS, 219, 12
Allart R., Lovis C., Pino L., Wyttenbach A., Ehrenreich D., Pepe F., 2017, A&A, 606, A144
Allende Prieto C., 2001, preprint (astro-ph/0111172)
Alonso-Floriano F. J. et al., 2019, A&A, 621, A74
Asplund M., Grevesse N., Sauval A. J., Scott P., 2009, ARA&A, 47, 481
Barman T. S., Konopacky Q. M., Macintosh B., Marois C., 2015, ApJ, 804, 61
Blanco-Cuaresma S., Soubiran C., Heiter U., Jofré P., 2014, A&A, 569, A111
Bourrier V. et al., 2018, A&A, 619, A1
Butler R. P., Marcy G. W., Williams E., Hauser H., Shirts P., 1997, ApJ, 474, L115
Casasayas-Barris N. et al., 2020, A&A, 635, A206
Charbonneau D., Brown T. M., Noyes R. W., Gilliland R. L., 2002, ApJ, 568, 377
Chen G. et al., 2018, A&A, 616, A145
Cosentino R. et al., 2012, Proc. SPIE, 8446, 84461V
Ehrenreich D. et al., 2012, A&A, 547, A18
Fischer D. A. et al., 2008, ApJ, 675, 790
Gardner J. P. et al., 2006, Space Sci. Rev., 123, 485
Gustafsson B., Edvardsson B., Eriksson K., Jørgensen U. G., Nordlund Å., Plez B., 2008, A&A, 486, 951

[8] https://petitradtrans.readthedocs.io/en/latest/

Hawker G. A., Madhusudhan N., Cabot S. H. C., Gandhi S., 2018, ApJ, 863, L11

Hoeijmakers H. J. et al., 2018, Nature, 560, 453

Hoeijmakers H. J. et al., 2019, A&A, 627, A165

McArthur B. E. et al., 2004, ApJ, 614, L81

Mahadevan S. et al., 2014, Proc. SPIE, 9147, 91471G

Malik M. et al., 2017, AJ, 153, 56

Malik M., Kitzmann D., Mendonça J. M., Grimm S. L., Marleau G.-D., Linder E. F., Tsai S.-M., Heng K., 2019, AJ, 157, 170

Marcy G. W., Butler R. P., Fischer D. A., Laughlin G., Vogt S. S., Henry G. W., Pourbaix D., 2002, ApJ, 581, 1375

Mayor M. et al., 2003, The Messenger, 114, 20

Mazeh T., Tamuz O., Zucker S., 2007, in Afonso C., Weldrake D., Henning T., eds, ASP Conf. Ser. Vol. 366, Transiting Extrasolar Planets Workshop. Astron. Soc. Pac., San Francisco, p. 119

Mollière P., Wardenier J. P., van Boekel R., Henning T., Molaverdikhani K., Snellen I. A. G., 2019, A&A, 627, A67

Moutou C., Boisse I., Hébrard G., Hébrard E., Donati J. F., Delfosse X., Kouach D., 2015, in Martins F., Boissier S., Buat V., Cambrésy L., Petit P., eds, SF2A-2015: Proceedings of the Annual meeting of the French Society of Astronomy and Astrophysics. Société Francaise d'Astronomie et d'Astrophysique (SF2A), Paris, p. 205

Nortmann L. et al., 2018, Science, 362, 1388

Nugroho S. K., Kawahara H., Masuda K., Hirano T., Kotani T., Tajitsu A., 2017, AJ, 154, 221

Parmentier V. et al., 2018, A&A, 617, A110

Pepe F. A. et al., 2010, Proc. SPIE, 7735, 77350F

Plez B., 2012, Astrophysics Source Code Library, record ascl:1205.004

Quirrenbach A. et al., 2016, Proc. SPIE, 9908, 990812

Rando N. et al., 2018, Proc. SPIE, 10698, 106980K

Rauer H. et al., 2014, Exp. Astron., 38, 249

Redfield S., Endl M., Cochran W. D., Koesterke L., 2008, ApJ, 673, L87

Ricker G. R., 2014, J. Am. Assoc. Var. Star Obser. (JAAVSO), 42, 234

Ridden-Harper A. R. et al., 2016, A&A, 593, A129

Ryabchikova T., Piskunov N., Kurucz R. L., Stempels H. C., Heiter U., Pakhomov Y., Barklem P. S., 2015, Phys. Scr., 90, 054005

Seidel J. V. et al., 2019, A&A, 623, A166

Sheppard K. B., Mandell A. M., Tamburo P., Gandhi S., Pinhas A., Madhusudhan N., Deming D., 2017, ApJ, 850, L32

Sousa S. G. et al., 2018, A&A, 620, A58

Stock J. W., Kitzmann D., Patzer A. B. C., Sedlmayr E., 2018, MNRAS, 479, 865

Tamuz O., Mazeh T., Zucker S., 2005, MNRAS, 356, 1466

Tsiaras A. et al., 2016, ApJ, 820, 99

Vogt S. S. et al., 1994, in Crawford D. L., Craine E. R., eds, Proc. SPIE Vol. 2198, Instrumentation in Astronomy VIII. SPIE, Bellingham, p. 362

Wildi F. et al., 2017, in Shaklan S., ed., Proc. SPIE Vol. 10400, Techniques and Instrumentation for Detection of Exoplanets VIII. SPIE, Bellingham, p. 321

APPENDIX A: EXTRA MATERIAL

Table A1. Observational time series for 55 Cnc. We provide Modified Julian Dates (MJD), radial velocities (RVs) for the Na I and Hα wavelengths and the effective resolution (in terms of FWHM) and the width of the convolution kernel (FWHM$_k$) for each individual exposure.

| MJD	t_{exp} (s)	RV (Na I) (km s^{-1})	FWHM (Na I) (km s^{-1})	FWHM$_k$ (Na I) (km s^{-1})	RV (Hα) (km s^{-1})	FWHM (Hα) (km s^{-1})	FWHM$_k$ (Hα) (km s^{-1})
58465.01122	900	27.79 ± 0.25	13.46 ± 0.14	5.12	27.72 ± 0.21	14.93 ± 0.15	4.43
58465.02281	900	27.53 ± 0.24	13.38 ± 0.13	5.32	27.57 ± 0.20	14.75 ± 0.15	5.02
58465.03939	900	27.40 ± 0.23	13.14 ± 0.13	5.89	27.50 ± 0.19	14.50 ± 0.15	5.7
58465.05083	900	27.22 ± 0.23	13.02 ± 0.13	6.15	27.43 ± 0.18	14.37 ± 0.14	6.02
58465.06241	450	27.28 ± 0.23	12.90 ± 0.13	6.40	27.51 ± 0.18	14.23 ± 0.14	6.34
58465.06864	450	27.29 ± 0.23	12.83 ± 0.13	6.54	27.44 ± 0.18	14.16 ± 0.14	6.50
58465.07487	450	27.41 ± 0.23	12.76 ± 0.13	6.67	27.51 ± 0.18	14.09 ± 0.14	6.65
58465.08109	450	27.60 ± 0.23	12.70 ± 0.13	6.79	27.71 ± 0.18	14.01 ± 0.14	6.82
58465.08732	450	27.72 ± 0.22	12.63 ± 0.13	6.92	27.85 ± 0.18	13.94 ± 0.14	6.96
58465.09354	450	27.91 ± 0.24	12.57 ± 0.13	7.02	27.73 ± 0.19	13.86 ± 0.14	7.16
58465.09975	450	27.93 ± 0.22	12.50 ± 0.13	7.15	28.00 ± 0.17	13.80 ± 0.14	7.23
58465.10598	450	28.01 ± 0.22	12.43 ± 0.12	7.27	28.16 ± 0.17	13.79 ± 0.14	7.25
58465.11480	450	28.10 ± 0.21	12.45 ± 0.12	7.23	28.23 ± 0.17	13.71 ± 0.14	7.40
58465.12101	450	28.14 ± 0.22	12.69 ± 0.13	6.81	28.16 ± 0.17	13.96 ± 0.14	6.91
58465.12724	450	28.20 ± 0.22	12.94 ± 0.13	6.32	28.27 ± 0.17	14.19 ± 0.14	6.43
58465.13347	450	28.14 ± 0.23	13.19 ± 0.13	5.78	28.17 ± 0.18	14.43 ± 0.14	5.87
58465.13969	450	28.05 ± 0.23	13.43 ± 0.13	5.20	28.10 ± 0.18	14.66 ± 0.15	5.27
58465.14591	450	28.07 ± 0.24	13.68 ± 0.14	4.50	28.05 ± 0.19	14.90 ± 0.15	4.55
58465.15214	450	28.13 ± 0.25	13.93 ± 0.14	3.65	28.13 ± 0.19	15.13 ± 0.15	3.72
58465.15836	450	28.25 ± 0.25	14.17 ± 0.14	2.56	28.19 ± 0.20	15.37 ± 0.15	2.55
58465.16730	450	28.44 ± 0.26	14.40 ± 0.14	0.00	28.41 ± 0.20	15.58 ± 0.16	0.00
58465.17353	450	28.43 ± 0.27	14.30 ± 0.14	1.69	28.36 ± 0.20	15.48 ± 0.16	1.76
58465.17975	450	28.30 ± 0.27	14.20 ± 0.14	2.39	28.24 ± 0.21	15.38 ± 0.15	2.49
58465.18598	450	28.15 ± 0.27	14.10 ± 0.14	2.92	28.00 ± 0.21	15.28 ± 0.15	3.04
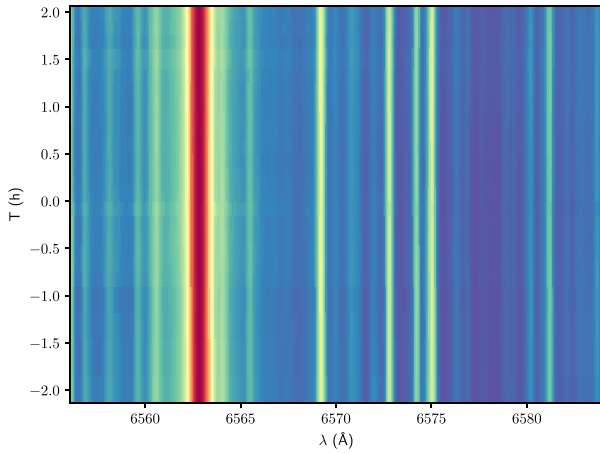
Figure A1. Same as Fig. 1, but for Hα.
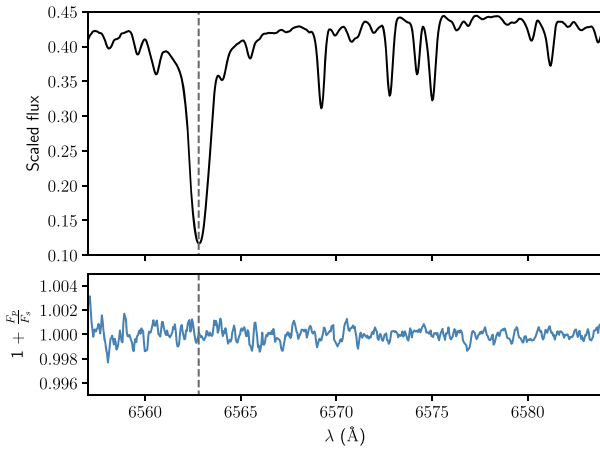
Figure A2. Final master stellar spectrum (top) and final transmission spectrum (bottom) for 55 Cnc e in the Hα region. The Hα wavelength is denoted by the vertical dashed line.
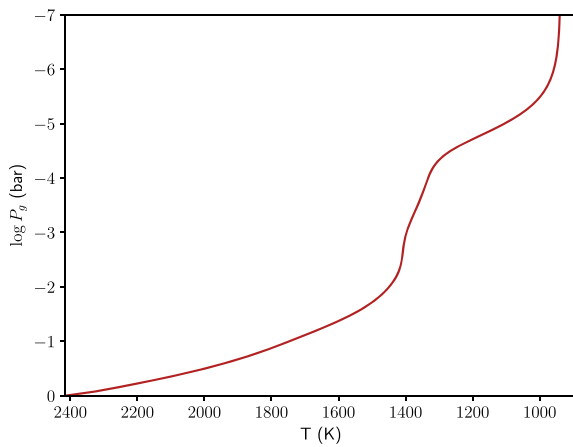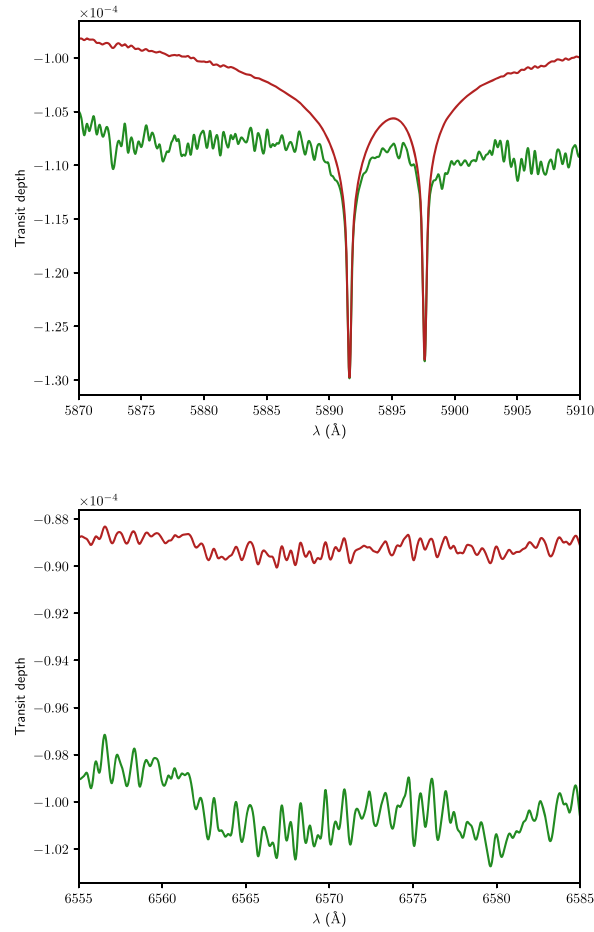

Figure A3. 55 Cnc e atmospheric *P*–*T* structure generated with the HELIOS code (Malik et al. 2017, 2019).
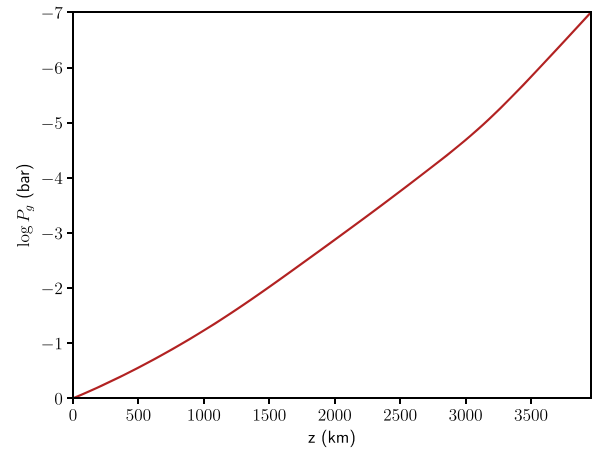
Figure A4. Same as Fig. A3, but for gaseous pressure as function of altitude (*z*).
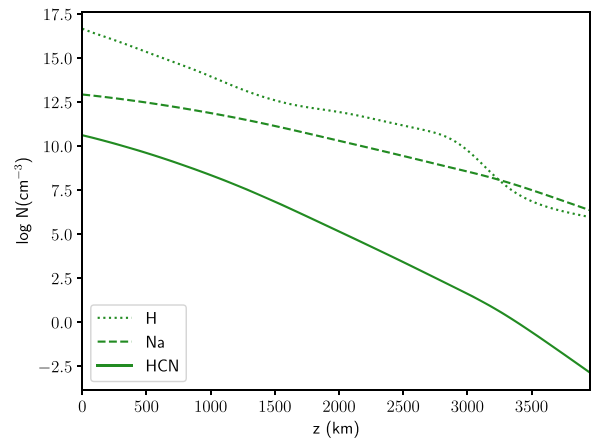
Figure A5. Number densities of H, HCN, and Na calculated with FASTCHEM (Stock et al. 2018) versus the model altitude (*z*). These number densities correspond to a model with a solar C/O ratio.

Figure A6. Our modelled synthetic spectra around Na I (top) and Hα (bottom) using PETITRADTRANS for the optical range. The green line corresponds to a model with a solar C/O ratio, whereas the red line represents twice the solar ratio. Both synthetic models have been degraded to the HORuS resolution as provided in Table A1.

This paper has been typeset from a TEX/LATEX file prepared by the author.